European Polymer Journal 229 (2025) 113876

Contents lists available at ScienceDirect

European Polymer Journal

journal homepage: www.elsevier.com/locate/europolj

Research Insights

Amphiphilic block copolymer conjugated with cell-penetrating-peptides derived from Influenza A H1N1 virus as a biocompatible scaffold for enhanced cell-uptake

Carolina Ventura-Hunter [a,b], David Pretzel [b,c,d], Carolin Kellner [b,c], Stephanie Hoeppener [b,c], Nicole C. Roesner [b,c], Patricia Quintana-Owen [e], Ulrich S. Schubert [b,c,d], Guadalupe Ayora-Talavera [f], Enrique Saldívar-Guerra [a,*], Stefano Fedeli [b,c,g,*], Carlos Guerrero-Sanchez [b,c,*]

[a] Department of Polymerization Processes, Centro de Investigacion en Química Aplicada (CIQA), Blvd. Enrique Reyna No. 140, 25294 Saltillo, Coahuila, Mexico
[b] Laboratory of Organic and Macromolecular Chemistry (IOMC), Friedrich Schiller University Jena, Humboldtstr. 10, 07743 Jena, Germany
[c] Jena Center for Soft Matter (JCSM), Friedrich Schiller University Jena, Philosophenweg 7, 07743 Jena, Germany
[d] Abbe Center of Photonics (ACP), Friedrich Schiller University Jena, Albert-Einstein-Straße 6, 07743 Jena, Germany
[e] Department of Applied Physics, CINVESTAV-IPN, Unidad Merida, A.P. 73, Cordemex, 97310 Merida, Yucatan, Mexico
[f] Laboratory of Virology, Regional Research Center Dr. Hideyo Noguchi, Universidad Autónoma de Yucatán, Av. Itzaes No. 490, Centro, 97000 Merida, Yucatan, Mexico
[g] Department of Pharmaceutical Sciences, Università degli Studi di Milano, Via G. Venezian 21, 20133 Milano, Italy

ARTICLE INFO

Keywords:
Amphiphilic copolymers
RAFT
Cell-penetrating peptides
Influenza A H1N1

ABSTRACT

Amphiphilic copolymers prepared by reversible addition-fragmentation chain-transfer (RAFT) polymerization are versatile and biocompatible scaffolds for multiple drug delivery applications. Decorating these structures with biomolecules and targeting moieties is a proven approach to enhance the cell uptake of polymers. In particular, spike proteins on the surface of the influenza A H1N1 virus are biomacromolecules highly evolved to promote cell adhesion and uptake, leading to effective cell-penetrating processes. We harnessed this uptake ability by selecting the peptide sequences responsible for the cell uptake and grafting them on a methacrylate copolymer. The adopted polymeric scaffold included glycerol, butyl, and N-hydroxy succinimide ester (NHS-ester) groups. This polymer resulted in a water-dispersible and biocompatible structure. Moreover, the reactivity of NHS-ester units enabled the modular insertion of the peptide in post-polymerization reactions. Through this approach, we combined the cell penetration efficiency of influenza A H1N1 virus with the easy manipulation of polymers and small biomolecules. The resulting bioconjugate was demonstrated to be a modular, safe, and effective platform for potential intracellular delivery applications.

1. Introduction

Amphiphilic copolymers represent versatile and robust platforms for drug delivery applications [1,2]. In this context, reversible addition-fragmentation chain-transfer (RAFT) polymerization offers a reliable technique for combining hydrophilic and hydrophobic monomers[3] into amphiphilic copolymers with different functions and properties [4]. These copolymers are dispersible in aqueous media and self-assemble into stable forms [5]. Incorporating reactive groups to the polymer backbone also enables post-polymerization modifications [6], which further expand the properties and applicability of these materials [7,8].

Amphiphilic copolymers can either chemically link or encapsulate bioactive compounds [9,10], producing nanocarriers that can enhance the cell-uptake of pharmaceutical payloads [11]. An essential aspect of these strategies is the ability of the polymeric scaffolds to penetrate targeted cells [12,13]. Decorating polymers with biomolecules such as biotin [14,15], folic acid [16,17], sugars [18,19], and proteic structures [20] has proven to improve cell penetration. Proteins and antibodies are particularly effective as they have domains that recognize cell receptors and enhance the internalization processes [21,22]. In this regard, cell-

* Corresponding authors.
E-mail addresses: enrique.saldivar@ciqa.edu.mx (E. Saldívar-Guerra), stefano.fedeli@unimi.it (S. Fedeli), carlos.guerrero.sanchez@uni-jena.de (C. Guerrero-Sanchez).

https://doi.org/10.1016/j.eurpolymj.2025.113876
Received 17 September 2024; Received in revised form 23 February 2025; Accepted 28 February 2025
Available online 1 March 2025

penetrating peptides are sequences of 5 to 30 amino acids that contain the essential recognition mechanisms of proteins [23], combining the efficacy developed by nature with the advantages of smaller biomolecules [24,25].

Harnessing viral proteins to mimic the innate cell-penetrating efficacy of viruses is a promising strategy for delivering bioactive compounds [26]. In particular, the surface of influenza A viruses present spike proteins evolved to promote cell adhesion and uptake [27], resulting in the virus phagocytosis and cell invasion [28]. However, manipulating proteins to decorate drug delivery systems presents various challenges [29]. Proteins can be easily denatured by temperature and pH variations as well as by contact with solid surfaces, resulting in loss of bioactivity [30]. Further difficulties account for protein isolation [31], low yields in the preparation of protein-polymer conjugates, and complex characterizations [32].

Influenza A virus H1N1 displays hemagglutinin spike proteins that recognize and penetrate target cells [33]. Specifically, these proteins recognize sialic acid molecules on the epithelial cells by interacting through the hemagglutinin receptor binding site [34]. Sialic acid is the terminal unit of several glycan structures that decorate the membrane of mammalian cells [35], offering an essential component for infections by influenza viruses [36]. The receptor binding site is composed of three conserved regions: the 130 (residues 135–138)- and 220 (residues 221–228)- loops and the 190-helix (residues 190–198) [37]. To identify potential cell-penetrating peptides, we considered the amino acid sequences of the hemagglutinin receptor binding site of the H1N1 virus from the vaccine strain A/California/07/2009 (H1N1pdm09). Building on these findings, we adopted these subunits as cell-penetrating peptides to decorate an amphiphilic block copolymer. Based on current examples of cell penetrating peptides conjugated to polymers, we propose to adopt the influenza A virus recognition motif to harness the viruses uptake efficiency in a biocompatible and versatile polymeric scaffold. We prepared an amphiphilic methacrylate-based block copolymer via RAFT polymerization, bearing hydrophilic and hydrophobic segments, and reactive *N*–hydroxy succinimide ester (NHS-ester) pendant groups. The nature of the polymer provided dispersibility in aqueous media via the formation of self-assembled polymeric nanoparticles (Fig. 1). Moreover, the NHS-ester sites allowed for the post-polymerization modification with the multivalent insertion of peptide sequences, promoting the effective polymer uptake [38].

Using the cell penetrating peptides derived from influenza A virus, we provided a preliminary study on a bioconjugate copolymer for intracellular delivery applications. We focused specifically on DSNKGVTAACPW, DQQSLYQNAW, and RPKVRDQEGRMW, analogs of the sequences 130, 190 and 220, and designated as PC1, PC2, and PC3, respectively. The tryptophan (W) end group was incorporated as a fluorescent moiety to quantify the functionalization degree of the peptide in the bioconjugates [39]. The cellular uptake of the 'pristine' peptides was also studied by adopting a fluorescein-conjugated form of the respective peptides (named PC1-5FAM and PC3-5FAM). Overall, we designed, synthesized, and characterized an amphiphilic block copolymer decorated with peptides, collecting groundwork data on the peptides biocompatibility and efficacy as cell-penetrating units. In addition, the physicochemical and *in vitro* properties of the investigated peptides were evaluated, offering a consistent rationale for the cell penetration data. Ultimately, our cell experiments demonstrated the effect of the peptide decoration on the polymer uptake.

2. Materials and methods

2.1. Materials

4-Cyano-4-(phenylcarbonothioylthio)pentanoic acid (CPAD, 97 % STREAM Chemicals), 4,4́-azobis(4-cyanopentanoic acid) (ACVA, ≥ 98 % Sigma-Aldrich), 1,1′-azobis(cyclohexanecarbonitrile) (V88, 98 % Sigma Aldrich), fluorescein-O-methacrylate (99 %, Sigma Aldrich), *N*-succinimidyl ester methacrylate (NHS-MA, > 98 %, TCI), triethylamine (TEA, 99.5 %, Sigma Aldrich), amino-2-propanol (93 %, Sigma-Aldrich),

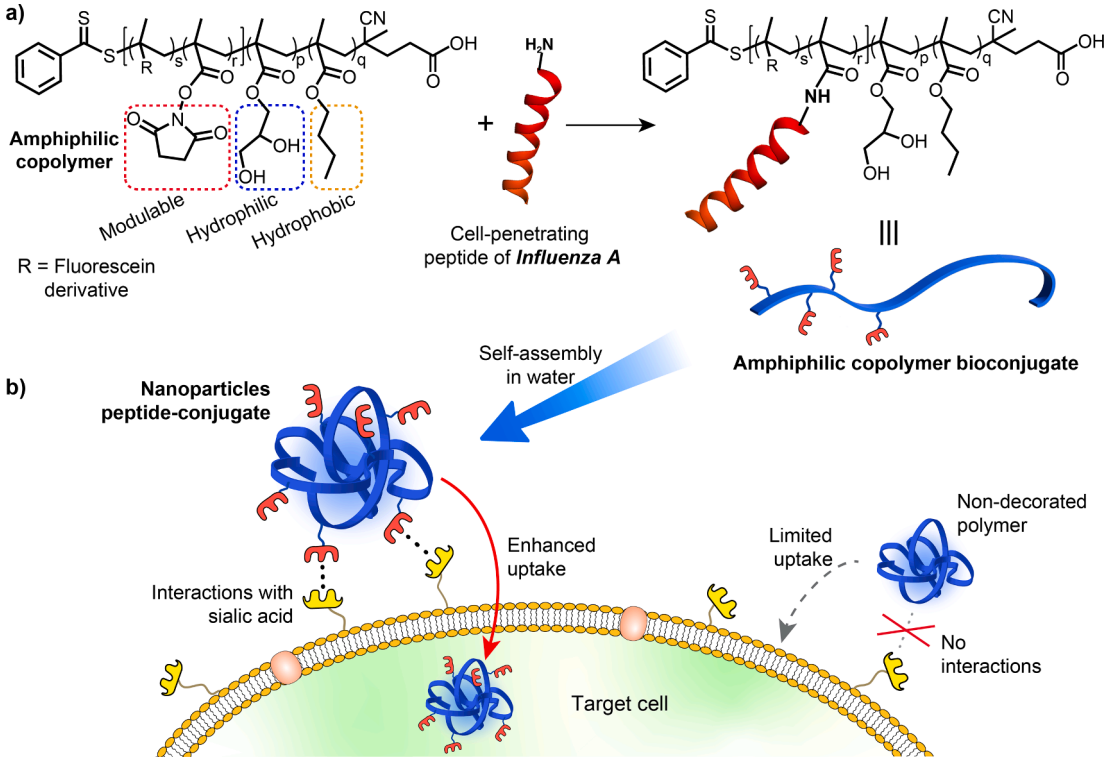

Fig. 1. A) schematic representation of the investigated amphiphilic block copolymer and its decoration with cell-penetrating peptides. b) the amphiphilic bioconjugate self-assembles into polymeric nanoparticles, enabling the stability in aqueous media and the enhanced cell uptake. note: the decoration yield was quantitative (> 98 %).

anisole (99 % Alfa Aesar), 1,4-dioxane (Alfa Aesar, anhydrous, 99.8 %), dimethyl sulfoxide (DMSO, anhydrous, ≥ 99.9 % Sigma-Aldrich) and 1,3,5-trioxane (≥ 99 % Aldrich) were used as received. Butyl methacrylate (BMA) (≥ 99 % Sigma-Aldrich) and glycerol methacrylate (glycerol-MA, 95 %, Polysciences, Inc) were purified by stirring in the presence of inhibitor remover beads (for hydroquinone and monomethyl ether hydroquinone, Sigma Aldrich). *N,N*-dimethylformamide (DMF) and dichloromethane (DCM) were obtained from a solvent purification system (MB-SPS-800 by MBraun) and stored under argon. PC1, PC2, PC3, PC1-5FAM and PC3-5FAM were purchased from Pepmic Co. (China).

2.2. Characterization methods

Size exclusion chromatography (SEC) of the polymers was performed on an Agilent system, equipped with a G1329A autosampler, a G1310A pump, a G1362A refractive index detector, and a PSS (Polymer Standards Service GmbH, Mainz, Germany) GRAM column with a solution of dimethylacetamide (DMAc) + 0.21 wt% LiCl as an eluent at a flow rate of 1 mL min^{-1} at 40 °C. The relative molar mass of the polymers was estimated against a calibration curve built with poly(methyl methacrylate) standards of narrow dispersity (*Đ*). Proton nuclear magnetic resonance (^{1}H NMR) spectroscopy was used to estimate the monomer conversion and the copolymer composition. The spectra were recorded at room temperature using a 300 MHz Bruker Avance I spectrometer equipped with a dual ^{1}H and ^{13}C probe head. Diffusion ordered spectroscopy (DOSY) experiments were measured on a 400 MHz Bruker Avance III spectrometer with a BBFO probe. The samples were measured in DMF-d_7, DMSO-d_6, and $CDCl_3$ at room temperature. A Zetasizer Nano ZS from Malvern Instruments (Herrenberg, Germany) was used for dynamic light scattering (DLS) investigations. The DLS was operated with a He–Ne laser at a wavelength of $\lambda = 633$ nm. The hydrodynamic diameter was approximated as the effective (z-average) diameter and the width of the distribution as the polydispersity index (PDI) of the nanoparticles obtained by the cumulants method and assuming a spherical particle model. Cryogenic transmission electron microscopic (cryo-TEM) images were acquired on a FEI Tecnai G2 20 TEM. Samples were prepared on Quantifoil grids (Quantifoil R2/2), which were hydrophilized prior to use via a treatment with Ar plasma for 2 min. 8.5 μL of the respective nanoparticle suspension were blotted onto the grid and plunged into liquid ethane, which served as a cryogen. The vitrification was performed with a Vitrobot Mark IV. After vitrification, the grids were transferred into a cryo-holder (Gatan 626) utilizing a Gatan cryo transfer stage and were measured at an acceleration voltage of 200 kV. Samples were maintained at a temperature below − 175 °C for all steps after the vitrification process. Images were recorded with a CCD camera system (Olympus Soft Imaging Systems, Megaview G2, 1376 × 1024 pixels). Fluorescence measurements (in solution and cell experiments) were recorded on a TECAN Infinite M200 Pro microplate reader.

2.3. Synthesis of the polymeric scaffold

The amphiphilic block copolymer (pBGF) was prepared from a poly (butyl methacrylate) (pBMA)-based macro chain transfer agent (CTA) (hydrophobic block) utilized for a chain extension reaction to incorporate the respective hydrophilic block.

2.3.1. Synthesis of the hydrophobic block (macro-CTA) (pBMA)

The pBMA homopolymer was synthesized as follows: BMA monomer (30 g, 210.97 mmol), CPAD RAFT agent (0.47 g, 1.68 mmol), V88 radical initiator (25.8 mg, 0.105 mmol) (BMA:CPAD:V88 = 125:1:0.06 mol ratio) and 1,3,5-trioxane internal standard (1.9 g, 21.10 mmol) were added into a 100 mL round-bottom flask. This solution was deoxygenated bubbling N_2 gas for 30 min and placed into an oil bath preheated at 90 °C. After 8 h, the reaction was quenched by cooling the flask into an ice bath. The monomer conversion was estimated to a value of 50 % via ^{1}H NMR analysis using 1,3,5-trioxane as an internal standard. The obtained polymer was precipitated into methanol (4x), filtered, and dried under vacuum at 40 °C for 48 h. The degree of polymerization (DP) and the number average molar mass (M_n) values of the purified polymer were estimated via ^{1}H NMR analysis, by comparing the integral values of the signals ascribed to the aromatic protons of the CPAD at 7.3–7.8 ppm to those of the methyl protons of the pBMA at 0.07–1.14 ppm (DP = 68, $M_{n,NMR} = 9900$ g mol^{-1}, $M_{n,theoretical} = 9100$ g mol^{-1}). SEC analysis yielded values of $M_{n,sec} = 9000$ g mol^{-1} and $Đ = 1.07$.

2.3.2. Synthesis of the amphiphilic block copolymer (pBGF)

The pBGF was prepared from the previously synthesized pBMA. The pBMA macro–CTA (1.92 g, 0.194 mmol), glycerol-MA monomer (1.87 g, 11.7 mmol), ACVA radical initiator (10.5 mg, 0.038 mmol), and 1,3,5-trioxane internal standard (117 mg, 1.32 mmol) were dissolved into 13 mL of DMF. This reaction mixture was cooled and deoxygenated bubbling N_2 gas for 30 min and placed into an oil bath preheated at 70 °C. After 3.5 h, 2 mL of a solution of DMF containing NHS–MA (255 mg, 1.39 mmol) and fluorescein *O*-methacrylate (22 mg, 0.055 mmol) (previously deoxygenated bubbling N_2 gas for 20 min) were added into the reaction mixture; this reaction step proceeded for 6.5 h at 70 °C. This copolymerization reaction was quenched by cooling the flask into an ice bath. The obtained copolymer was dialyzed against acetone and dried under vacuum at 40 °C for 48 h (Spectra/Por® regenerated cellulose membrane, Spectrum Labs, MWCO = 3.5 kDa, compatible with multiple solvents). The monomer conversions were estimated via ^{1}H NMR analysis using 1,3,5-trioxane as an internal standard (i.e., 58 % for the glycerol-MA (signals at 5.5 ppm and 6.4 ppm) and 65 % for the NHS–MA (signals at 5.8 and 6.8 ppm)). The NHS–MA content in the copolymer was also consistent with the value estimated via elemental analysis (~2.68 units per chain). Glycerol–MA units were determined via a quantitative ^{13}C NMR method (Inverse-Gated Decoupling) using DMF-d_7 and by comparing the integral values of BMA signals at 64.69 ppm (–COO–$\underline{C}H_2$–CH_2–) with that of the signals ascribed to glycerol–MA at 63.60 ppm (–COO–CH_2–CHOH-$\underline{C}H_2$OH), 66.78 ppm (–COO–$\underline{C}H_2$–CHOH-CH_2OH) and 69.88 ppm (–COO–CH_2–$\underline{C}$HOH-CH_2OH); $DP_{glycerol\text{-}MA} = 31$. $M_{n,NMR} = 15400$ g mol^{-1} was determined using the DP values obtained for glycerol–MA and NHS–MA co-monomers. $M_{n,theoretical} = 16500$ g mol^{-1} was calculated using monomer conversion as obtained via ^{1}H NMR analysis. SEC analysis yielded values of $M_{n,sec} = 20500$ g mol^{-1} and $Đ = 1.13$.

2.3.3. Synthesis of the peptide-bioconjugated copolymers

Peptides PC1 (loop 130, sequence: DSNKGVTAACPW) and PC3 (loop 220, sequence: RPKVRDQEGRMW) were conjugated to copolymer pBGF via an ester activation procedure. The corresponding peptide (PC1 (21.8 mg, 17.51 μmol) or PC3 (18.7 mg, 12.05 μmol)) and triethylamine (15 μL, 107.64 μmol) were dissolved in 2 mL of DMF in a glass vial. This solution was deoxygenated for 15 min bubbling N_2 gas and added dropwise into another glass vial containing the copolymer pBGF (200 mg, 37.66 μmol) dissolved in 1 mL of deoxygenated DMF under magnetic stirring. The polymer–peptide solution was placed into an oil bath preheated at 50 °C. After 24 h, amino-2-propanol (8 μL, 103 μmol) was added into the vial and this reaction step proceeded for 12 h. The conjugated polymers were purified via dialysis against water for 48 h (Spectra/Por® regenerated cellulose membrane, Spectrum Labs, MWCO = 3.5 kDa, compatible with multiple solvents) to remove the unreacted peptide, and lyophilized yielding 70 mg of product.

2.4. Evaluations of potential cytotoxic effects of peptides and peptide-polymer conjugates

The potential cytotoxicity of the materials was investigated using the Madin-Darby Canine Kidney (MDCK) and HEPG2 cell lines following the standardized procedure described in the ISO10993-5 guideline. The

Dulbeccós Modified Eagle Medium (DMEM) Nutrient Mixture F12 supplemented with 10 % fetal calf serum, 100 U mL^{-1} penicillin, and 100 mg mL^{-1} streptomycin (Biochrom, Berlin, Germany) was used as a culture media. Cells were routinely cultured at 37 °C in a humidified atmosphere containing 5 % CO_2. Cells were plated at a density of 10^4 cells per well in 96-well plates and grown for 24 h. After 24 h, culture media was replaced by fresh media containing the dissolved peptides or the polymer-conjugates. Control cells were incubated with fresh culture medium. After additional 24 h of incubation, media was removed, cells were washed with phosphate buffered saline (PBS) and subsequently treated with PrestoBlue reagent diluted in culture medium according to the instructions of the manufacturer (Invitrogen, Germany). After 45 min of incubation at 37 °C, fluorescence of the media was measured at the wavelengths of Ex 560/Em 590 nm. Samples displaying a cell viability value higher than 70 % were considered as non-cytotoxic. Experiments were performed in sextuplicate.

2.5. Cell-uptake experiments and flow cytometry quantification

The cellular uptake of the bioconjugates was determined via flow cytometry using MDCK cells plated in 12-well plates at a density of 10^5 cells per well. After 24 h, culture media was replaced by fresh media containing the dissolved peptides or the polymer-conjugates. Control cells were incubated with fresh culture medium. Cells were incubated for additional 24 h, washed with PBS, harvested by trypsinization and resuspended in PBS supplemented with 10 % fetal calf serum. To determine the relative uptake of the bioconjugates, 10^4 cells were quantified via flow cytometry using a Cytoflex S (Beckman Coulter) and the 488 nm laser for excitation and the FITC filter set for detection of the emission signal. For microscopic analysis, the cell nuclei were additionally stained with media containing Hoechst 33342 dye (10 mg mL^{-1}) for 10 min, and after once washing with media immediately subjected to fluorescence imaging.

3. Results and discussion

3.1. Design and synthesis of the amphiphilic block copolymer

For producing a water-soluble amphiphilic polymer with functional groups suitable for post-polymerization modifications, we focused on a poly(methacrylate) hydrophilic/hydrophobic block copolymer prepared via the RAFT technique. The hydrophobic block was composed of pBMA, while the hydrophilic segment contained a mixture of three methacrylate derivatives: glycerol, fluorescein, and NHS-ester. The glycerol units featured a hydrophilic nature, while the NHS-ester units introduced reactive sites for the peptide conjugation. In due course, the fluorescein units are easy to incorporate onto the polymer chains via copolymerization of their (meth)acrylate derivatives and enable tracking of the polymer in the different bioenvironments [40]. Thus, the polymer scaffold (pBGF) was prepared by first synthesizing the hydrophobic block (pBMA) and subsequently performing a chain extension reaction to add the hydrophilic part (Scheme 1). This combination of selected monomers led to an amphiphilic and biocompatible material that can be stably dispersed in aqueous media. Furthermore, it is known that polymers of certain molar mass can improve the bioavailability and activity of different biomolecules [41].

The RAFT polymerization of BMA yielded the hydrophobic block pBMA, which also served as macro-CTA for the subsequent chain extension reaction with the hydrophilic monomers. This first polymerization proceeded up to 50 % monomer conversion yielding a pBMA macro-CTA with a DP value of 68 ($M_{n,NMR}$ = 9900 g mol^{-1}; SEC analysis: $M_{n,sec}$ = 9000 g mol^{-1} and $Đ$ = 1.07; see Fig. S1 and Fig. S5). During the subsequent chain extension, the utilized monomers were fed at different times (see Materials and methods section for details). Glycerol–MA was first polymerized and subsequently a mixture of NHS-MA and fluorescein *O*–methacrylate. The conversion obtained after the first glycerol-MA polymerization was 58 % to yield a total DP value of 31. The deferred feed of this latter monomer mixture enabled the segregation of the NHS-ester and fluorescent units toward the end of the copolymer chain (in the hydrophilic segment). In previous studies, we demonstrated how the radical chain end of this reaction has no preference for adding either glycerol-MA or NHS-MA units [42]. The final composition was a terpolymer formed by a hydrophobic block followed by a hydrophilic portion. This composition offered a water-soluble structure with better chances to self-assembly into stabilized nanoparticles. The segregated incorporation of NHS-ester at the hydrophilic segment also presented more exposed sites for the bioconjugation reaction. Eventually, the more exposed peptide and fluorescent units are expected to be more available for interactions with cells and fluorescence investigations. The final copolymer was characterized via ^{1}H NMR, ^{13}C NMR, SEC, and elemental analysis ($M_{n,NMR}$ = 15400 g mol^{-1}, $Đ$ = 1.13 (see Fig. S2 to Fig. S5).

3.2. Characterization of the peptides

The physicochemical properties of the investigated peptides were estimated using the ProtParam tool in the Expasy server (https://web.expasy.org/protaram/). Results (see Tab. S1) suggest a prevalent hydrophilic nature of the peptides, with an isoelectric point value of 5.83,

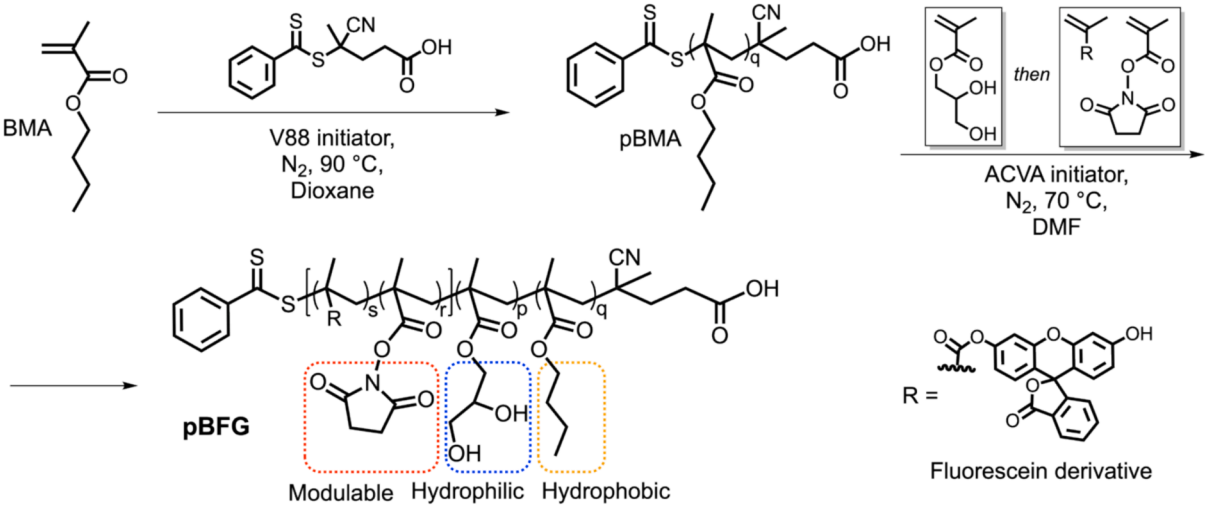

Scheme 1. Schematic representation of the synthesis of the amphiphilic block copolymer pBGF, s = 0.1, r = 3, p = 30, q = 68.

3.8, and 10.74 for PC1, PC2, and PC3, respectively. We calculated the secondary structures of the peptides using two online computational tools: *PEP-FOLD3*[43] and *I-TASSER* [44]. These models (Fig. 2a) estimated a mostly coiled conformation for peptides PC1 and PC3, and a predominant α-helix conformation for peptide PC2. Variations in the confidence scores were expected (numbers 0–9 in Fig. 2a), reflecting the prediction reliability for any given position. The tridimensional structures were predicted with the aid of *PEP-FOLD3*, confirming an α-helix conformation dominant for PC2 and for most of PC3, but absent for PC1 (Fig. 2b). The prediction profile of the local structure was also obtained with the aid of *PEP-FOLD3* and agreed with the other calculations [45,46]. These latter predictions confirmed a higher probability of finding an α-helix structure for PC2 as compared to peptides PC1 and PC3 (Fig. 2c). Overall, these computational data for PC1 and PC2 are consistent with the original conformation of the hemagglutinin protein, where these sequences are, indeed, part of a coiled and an α-helical structure, respectively. In contrast, the prediction for PC3 suggests a prevalent α-helical structure, but in the original protein is mostly as a coil. Even though this preliminary theoretical assessment offered a good starting point to elucidate the secondary structure of the investigated peptides, experimental evaluations (e.g., circular dichroism (CD) spectroscopy or other techniques) might confirm these findings and also provide additional information for a deeper understanding of their actual conformation;[47] these fundamental investigations might be reported in future research work.

As aforementioned, all the investigated peptides contained a terminal tryptophan unit as a fluorescent moiety. These fluorophores facilitated the evaluation of the degree of conjugation between the peptide and the polymer scaffold. As a reference, each peptide was also characterized via NMR and fluorescence spectroscopy (see Fig. S6 to S10). In this regard, peptide PC2 had a low solubility in PBS and, therefore, its fluorescence analysis in aqueous media was not feasible. Besides this limitation, PC2 also showed a certain degree of cytotoxicity (see Fig. S12). For these reasons, PC2 was not further considered for conjugation reactions with the polymer scaffold. The fluorescence properties of all investigated compounds were analyzed using three-dimensional excitation-emission matrix (3D-EEM) spectroscopy (see Fig. S13 to S16 and Tab. S2). This technique simultaneously scans different excitation and emission wavelengths, providing comprehensive information about the fluorescence distribution and intensity[49].

3.3. Conjugation of polymer scaffold with the peptides

The decoration of pBGF with the cell-penetrating peptides PC1 and PC3 derived from the influenza A virus yielded two water-dispersible and biocompatible vectors with the potential capability to display an enhanced cell penetration. The peptides were linked to the pBGF copolymer via a *grafting to* method performed at 50 °C for 24 h (Scheme 2). The selection of glycerol-MA and NHS-MA comonomers was based on their capability to provide a biocompatible scaffold and reactive sites for the peptide insertion, respectively, which provides good candidate vectors for nanomedicine applications [50].

The conjugation reaction between the polymer scaffold and the biomolecules was analyzed via DOSY-NMR experiments. This technique analyzes the diffusion coefficient (*D*) of the different signals *vs.* the monodimensional ^{1}H NMR spectrum[51] (detailed 1H spectrum in Fig. S11). Thus, signals derived from the same macromolecule will have the same *D* values lying on the same horizontal line in the corresponding plot, while signals of different molecules will have different *D* values and will lay on distinct lines. Hence, this technique can discriminate between

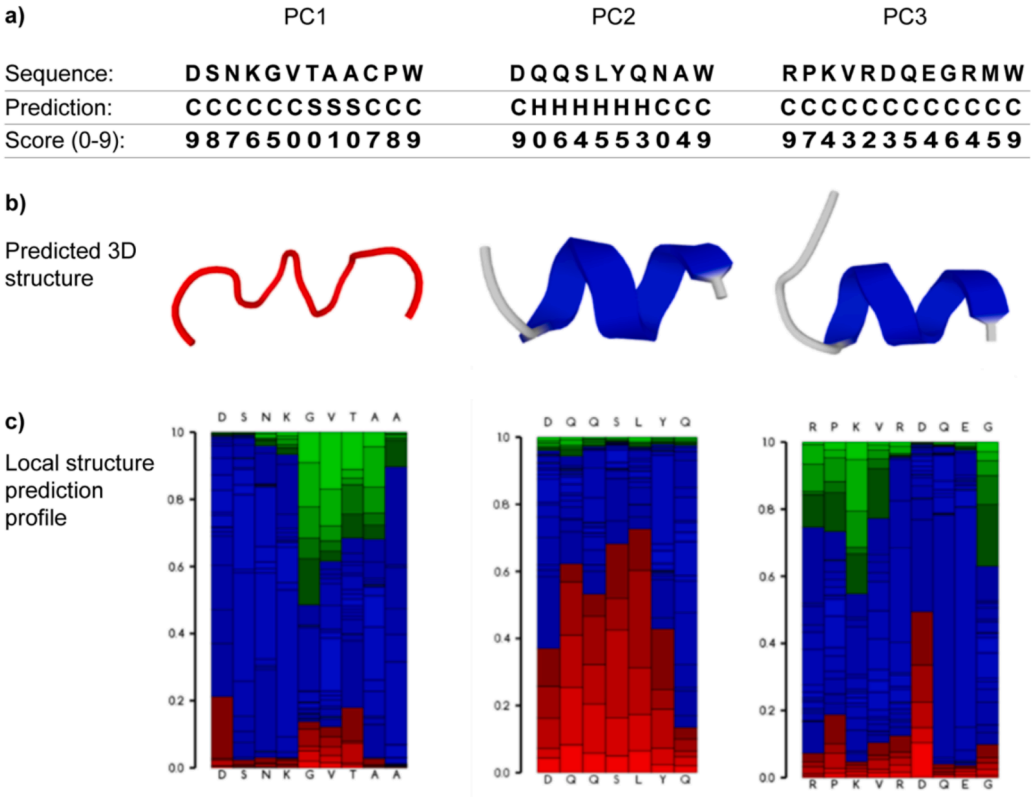

Fig. 2. Secondary structure of the investigated peptides generated with the aid of PEP-FOLD3 and I-TASSER platforms. a) Prediction of the secondary structure and confidence scores. Values indicate the confidence level in the expected structure of the corresponding sequence of amino acids. 0 = less confident, 9 = most confident. H = α-helix, S = strand, C = coil. (computed by I-TASSER, Zhang Lab, University of Michigan, 2018) [48]. b) Three-dimensional models predicted by the PEP-FOLD3 platform using 100 simulations. c) Local structure predictions generated with the aid of the PEP-FOLD3 platform; color code: red = helical, green = extended, and blue = coil.

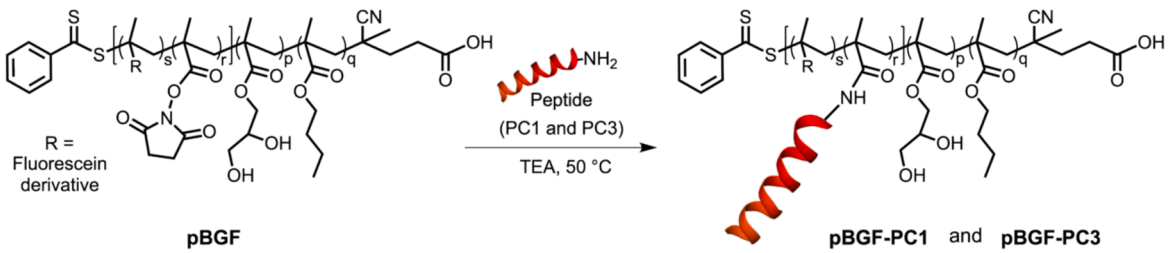

Scheme 2. Schematic representation of the conjugation method between the cell-penetrating peptides derived from influenza A spike protein hemagglutinin and the proposed amphiphilic block copolymer. Note: the conjugation yield was >98 % with PC1 and ~ 30 % with PC3.

mixtures of precursor compounds and conjugated structures [52]. We thus analyzed the precursor copolymer scaffold (Fig. 3a), the pristine peptides (Fig. 3b and 3d), and the corresponding products (Fig. 3c and 3e). The presence of the signals in the range from 6.6 to 8 ppm at the *D* values of the polymer (orange dashed line) in samples pBGF–PC1 (Fig. 3c) and pBGF-PC3 (Fig. 3e) suggests the formation of a covalent bond between the pBGF polymer scaffold and peptides PC1 and PC3, respectively. The conjugation reactions were confirmed by the absence of NMR signals at the *D* values of the pristine peptides (green dashed line) in the spectrum of the corresponding products. It is worth noting that the *D* value of the conjugates is slightly varied with respect to the polymer precursor; this effect can be explained by the incorporation of the peptides into the polymer scaffold, which result in altering the molar mass of the material and the hydrodynamic radius of the polymer chains [52]. When peptides or proteins are conjugated to polymers, additional interactions between such biomolecules and the polymer chains have been observed as reported elsewhere [53–55]. Hence, the secondary structure of proteins or peptides might be altered as a consequence of experienced changes in their new chemical environment (e.g., modifications/formation of hydrogen bonds and /or steric hindrances). For the bioconjugates synthesized in this contribution, interactions between the selected peptides and the hydrophilic segment of the polymer scaffold bearing methacrylate and hydroxyl moieties may, indeed, have an influence on the secondary structure of the peptide. This is, indeed, a very interesting situation demanding for further and more detailed investigations, which will be definitively considered in future research

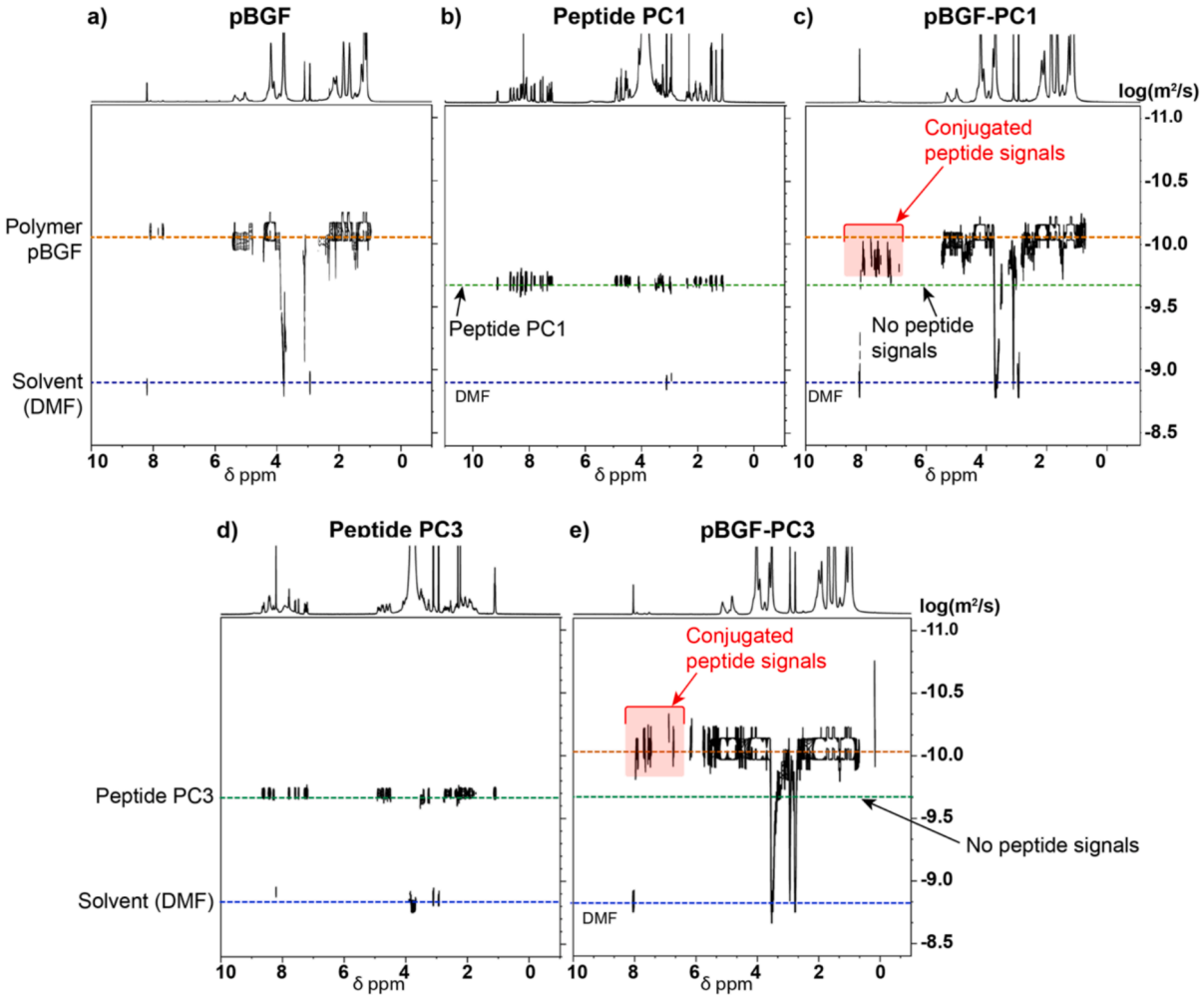

Fig. 3. 2D DOSY spectra of the reagents and products of the conjugation reactions. The analyses were performed in DMF-d_7 (400 MHz, RT). a) pBGF (copolymer precursor). b) Peptide PC1. c) Conjugate pBGF-PC1. d) Peptide PC3. e) Conjugate pBGF-PC3. Note: the y-axes on the right are aligned and the same for all the plots.

work.

The peptide content in the conjugates was determined by quantifying the tryptophan fluorescence (*i.e.*, emission). The estimation of the degree of conjugation was obtained considering the precursor NHS-ester sites and the final peptide units quantified through calibration curves built at the wavelength values of $\lambda_{Ex} = 280$ nm and $\lambda_{Em} = 340$ nm (see Figs. S17 to S19, Tab. S3, and Tab. S4). The results showed a quantitative decoration (98.1 %) for pBGF-PC1, while only around 31.5 % for pBGF-PC3 (Tab. S3). The low incorporation of PC3 into the polymer scaffold may be attributed to a slower reaction rate of this peptide combined with the time-sensitive reactivity of NHS-ester towards hydrolysis. Possible side-reactions with the glycerol groups can have also contributed to the NHS-ester consumption overt time [56].

Both precursor polymer scaffold and derived conjugates dispersed in aqueous media and formed self-assembled nanostructures. These structures are consistent with the amphiphilic nature of the copolymer chains [57]. The obtained dispersions were analyzed via DLS and presented different hydrodynamic diameters: the size was around 100 nm for pBGF and pBGF–PC3, while 10 nm for pBGF-PC1 (Fig. 4a DLS). These distinct sizes can be explained with the substantial different conjugation degree of pBGF-PC1 with respect to pBGF-PC3. The multivalent peptide-decoration is expected to improve the hydrophilicity of the polymer and, therefore, its dispersibility, while being less prone to form aggregated polymer chains [58]. The observed size of 10 nm suggested a predominant arrange of the polymer molecules into single–chain polymeric nanoparticles[59] similar to that of other water-soluble polymers with a peptide decoration [60]. The relatively low degree of conjugation of pBGF-PC3 eventually offered a rationale for the nanoparticle size comparable to that of the unconjugated polymer precursor. Cryo-TEM investigations confirmed the presence of these different self-assembled nanostructures with size and micellar morphology co-existing with vesicles (Fig. 4b).

3.4. Biocompatibility of the conjugated polymers and peptides, and cell uptake investigations

The biocompatibility of the investigated peptides and fluorescent derivatives was tested using epithelial MDCK cells. The MDCK model was selected due to the significant expression of sialylated proteins on the cell membrane, which might contribute to maximize interactions with the investigated peptides [61]. The results revealed low cytotoxic effect up to a concentration of 125 μg mL^{-1}; even a slightly lower cytotoxicity was observed for the non-fluorescent peptides (Fig. 5a).

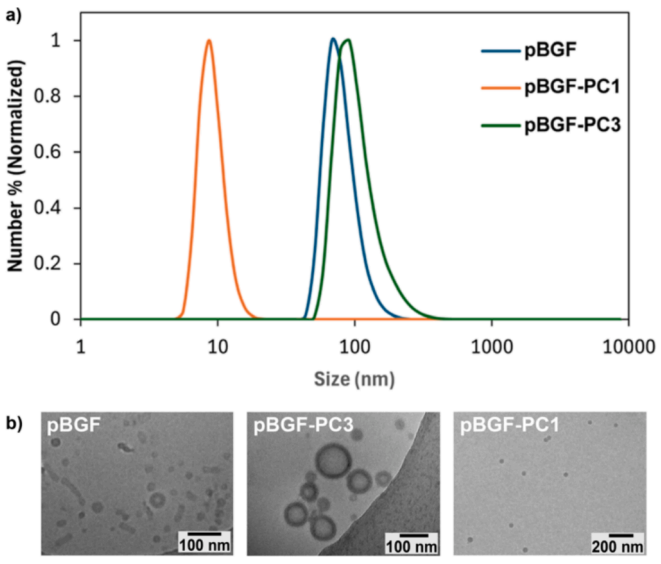

Fig. 4. A) dls analyses of aqueous dispersions of the precursor polymer scaffold and conjugated materials. b) related cryo-tem analyses.

Likewise, the biocompatibility of the bioconjugates was tested using MDCK cells incubated for 24 h at two different concentrations: 100 and 200 μg mL^{-1}. We also investigated possible specific toxicity of the polymer structures on hepatic cells [62], adopting the HepG2 line as an in vitro model of liver cells [63]. As observed in Fig. 5b, results revealed a mostly safe profile of the investigated copolymer and bioconjugates.

Ultimately, we tested the cellular uptake of the peptides and polymer conjugates via the quantification of the internalized material by flow cytometry. To evaluate the uptake of the pristine peptides, we examined a fluorescein-decorated version of PC1 and PC3 (PC1-5FAM and PC3-5FAM). These fluorescent peptides showed a dose-dependent cell uptake for both PC3-5FAM and PC1-5FAM (Fig. 6a), with even distribution in the cytoplasm and nucleus (Fig. S20) that point to a cytosolic delivery [64,65]. These results strongly suggest that the peptides proposed herein may be good alternatives to other well-investigated cell penetrating peptides such as those derived from human calcitonin utilized in MDCK-based models [66,67], which, at some extent, have shown cell penetrating properties [68], but certain limitations as systemic drug delivery vehicles [69]. In turn, the bioconjugate polymer pBGF-PC1 showed a significantly higher cellular uptake than its counterparts pBGF and pBGF-PC3, being these latter two comparable (Fig. 6b). This outcome was consistent with the difference in the degree of functionalization of the two bioconjugate polymers. Furthermore, size-related contributions to the uptake cannot be totally excluded; however, the substantial disparity in the peptide decoration –around 31.5 % for pBGF-PC3, while practically quantitative for pBGF-PC1– suggested the effective contribution of peptide PC1 in promoting the internalization of the polymer. We observed no strict concentration-dependent uptake of the peptide-polymer conjugates. This difference with respect to free peptides can be explained considering the distinct internalization rate of bioconjugates [70], requiring significantly longer incubation times to be comparable to those found for smaller peptides [71]. These *in vitro* experiments showed the contribution of the grafted peptides on the internalization of the pBGF PC1, presenting the biocompatibility and enhanced cell-penetration of this bioconjugate amphiphilic copolymer.

4. Conclusion

In summary, we developed an amphiphilic copolymer modulable through a "*grafting to*" conjugation with cell-penetrating peptides of influenza A virus. These peptides were chosen from the hemagglutinin spike protein of the virus, selecting the key amino acid sequences that recognize the sialic acid receptors and penetrate the cell membrane. The amphiphilic copolymer was prepared via the RAFT technique, combining hydrophobic, hydrophilic, and NHS-ester methacrylate monomers. We also added a fluorescein-derivative monomer to track the copolymer in *in vitro* studies. The copolymer resulted in an amphiphilic scaffold with self-assembly capability in aqueous media and with reactive sites for peptide grafting. The post–polymerization modification yielded a highly water-soluble structure with a multivalent peptide decoration. The chemical-physical properties of this bioconjugate were characterized and tested *in vitro,* showing a highly biocompatible material with enhanced cell penetration performance. Overall, this strategy combined the cell–penetration efficiency of viruses with the easy manipulation of polymers and small biomolecules. These reported investigations on cellular uptake and self-assembly represent a promising starting point for testing drug delivery strategies. By acting as surfactant this bioconjugate is likely expected to form self-assemblies with lipophilic drugs, enhancing their water dispersibility and cell internalization. Additionally, the modularity of the post-polymerization offers possibilities for further optimizations, presenting an efficient and versatile platform for future studies in cell-penetrating applications.

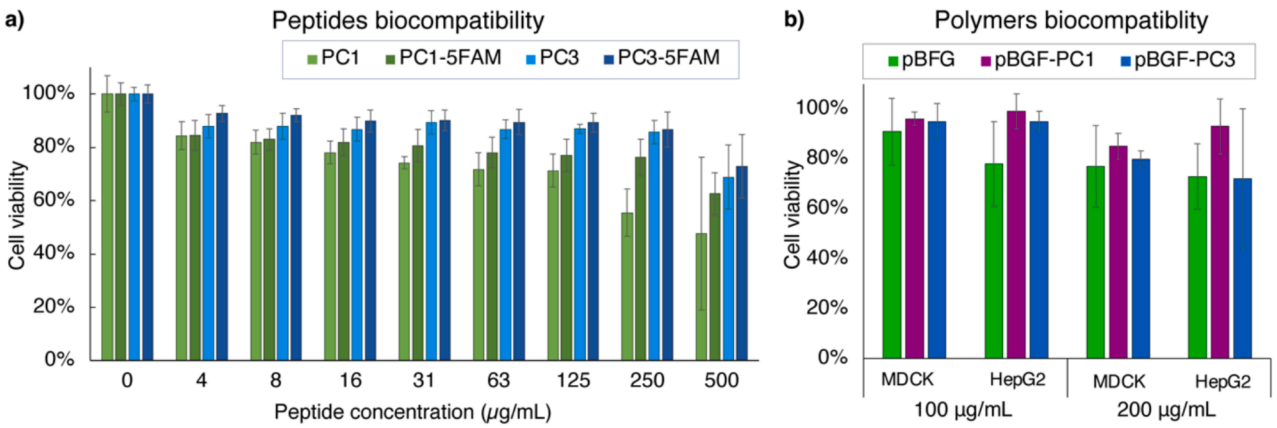

Fig. 5. Cytotoxicity of: a) peptides on MDCK cells and b) polymeric materials on MDCK and HepG2 cell lines.

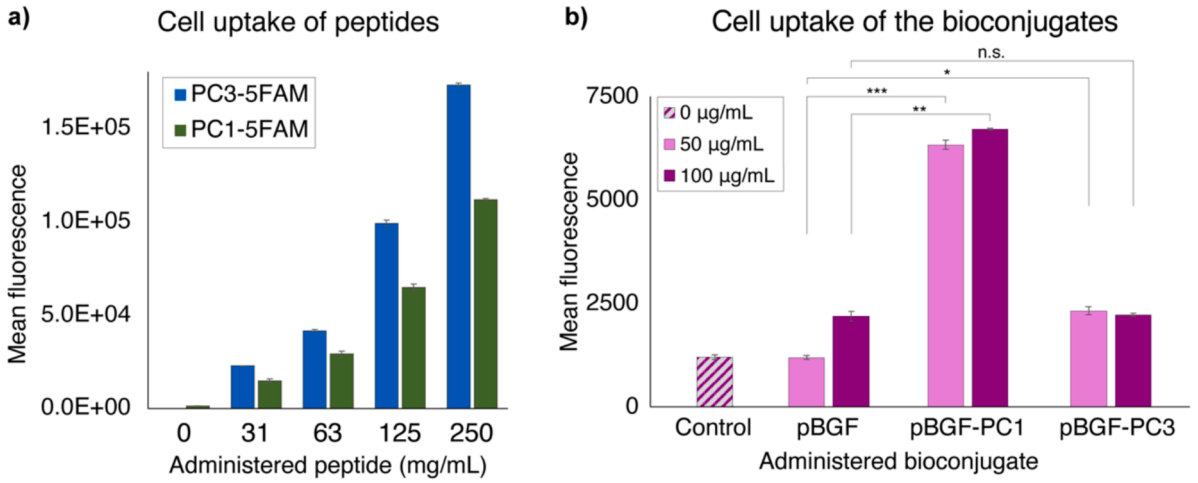

Fig. 6. Uptake experiments for MDCK cells. a) Fluorescent peptides. b) Polymer bioconjugates. *: $p \leq 0.05$, **: $p \leq 0.01$, ***: $p \leq 0.005$.

CRediT authorship contribution statement

Carolina Ventura-Hunter: Writing – review & editing, Writing – original draft, Visualization, Validation, Software, Methodology, Investigation, Formal analysis, Data curation. **David Pretzel:** Writing – review & editing, Visualization, Validation, Software, Formal analysis, Data curation. **Carolin Kellner:** Writing – review & editing, Visualization, Validation, Software, Investigation, Formal analysis, Data curation. **Stephanie Hoeppener:** Writing – review & editing, Visualization, Validation, Software, Investigation, Formal analysis, Data curation. **Nicole C. Roesner:** Writing – review & editing, Visualization, Data curation. **Patricia Quintana-Owen:** Writing – review & editing, Supervision, Resources, Project administration, Funding acquisition, Conceptualization. **Ulrich S. Schubert:** Writing – review & editing, Resources, Project administration, Funding acquisition. **Guadalupe Ayora-Talavera:** Writing – review & editing, Supervision, Resources, Project administration, Funding acquisition, Conceptualization. **Enrique Saldívar-Guerra:** Writing – review & editing, Supervision, Resources, Project administration, Funding acquisition, Conceptualization. **Stefano Fedeli:** Writing – review & editing, Writing – original draft, Visualization, Validation, Supervision, Formal analysis, Data curation, Conceptualization. **Carlos Guerrero-Sanchez:** Writing – review & editing, Supervision, Resources, Project administration, Investigation, Funding acquisition, Formal analysis, Conceptualization.

Declaration of competing interest

The authors declare that they have no known competing financial interests or personal relationships that could have appeared to influence the work reported in this paper.

Acknowledgements

C.V.-H. thanks the Fondo para la Investigacion Científica y Tecnologica (FONCYT, Mexico) and the Consejo Estatal de Ciencia y Tecnología del Estado de Coahuila (COECYT, Mexico, grant COAH-2019-C13-B02) for funding. The authors acknowledge the financial support of the Consejo Nacional de Humanidades, Ciencias y Tecnologías (CONAHCyT, Mexico) through a Ph. D. scholarship (C.V.-H.) and project CB-2015/253303. This work was also financially supported by the Deutsche Forschungsgemeinschaft (DFG, Germany) Collaborative Research Center 1278 “PolyTarget” (project number 316213987; projects B02 and Z01). The authors thank Jens Ulbrich for his support in the laboratory.

Appendix A. Supplementary data

Supplementary data to this article can be found online at https://doi.org/10.1016/j.eurpolymj.2025.113876.

Data availability

Data will be made available on request.

References

[1] A. Rösler, G.W.M. Vandermeulen, H.-A. Klok, Advanced drug delivery devices via self-assembly of amphiphilic block copolymers, Adv. Drug Deliv. Rev. 64 (2012) 270–279, https://doi.org/10.1016/j.addr.2012.09.026.

[2] A. Aliabadi, M. Hasannia, M. Vakili-Azghandi, F. Araste, K. Abnous, S.M. Taghdisi, M. Ramezani, M. Alibolandi, Synthesis approaches of amphiphilic copolymers for spherical micelle preparation: application in drug delivery, J. Mater.chem B 11 (2023) 9325–9368, https://doi.org/10.1039/D3TB01371E.

[3] G. Moad, RAFT polymerization to form stimuli-responsive polymers, Polym. Chem. 8 (2017) 177–219, https://doi.org/10.1039/C6PY01849A.

[4] C. Lu, M.W. Urban, Stimuli-responsive polymer nano-science: Shape anisotropy, responsiveness, applications, Prog. Polym. Sci. 78 (2018) 24–46, https://doi.org/10.1016/j.progpolymsci.2017.07.005.

[5] F. D'Agosto, J. Rieger, M. Lansalot, RAFT-Mediated Polymerization-Induced Self-Assembly, Angew. Chem. Int. Ed. 59 (2020) 8368–8392, https://doi.org/10.1002/anie.201911758.

[6] B.D. Fairbanks, P.A. Gunatillake, L. Meagher, Biomedical applications of polymers derived by reversible addition – fragmentation chain-transfer (RAFT), Adv. Drug Deliv. Rev. 91 (2015) 141–152, https://doi.org/10.1016/j.addr.2015.05.016.

[7] M.A. Gauthier, M.I. Gibson, H. Klok, Synthesis of Functional Polymers by Post-Polymerization Modification, Angew. Chem. Int. Ed. 48 (2009) 48–58, https://doi.org/10.1002/anie.200801951.

[8] J. Rieger, Guidelines for the Synthesis of Block Copolymer Particles of Various Morphologies by RAFT Dispersion Polymerization, Macromol. Rapid Commun. 36 (2015) 1458–1471, https://doi.org/10.1002/marc.201500028.

[9] W. Zhang, C. Hong, C. Pan, Polymerization-Induced Self-Assembly of Functionalized Block Copolymer Nanoparticles and Their Application in Drug Delivery, Macromol. Rapid Commun. 40 (2019) 1800279, https://doi.org/10.1002/marc.201800279.

[10] H. Phan, V. Taresco, J. Penelle, B. Couturaud, Polymerisation-induced self-assembly (PISA) as a straightforward formulation strategy for stimuli-responsive drug delivery systems and biomaterials: recent advances, Biomater. Sci. 9 (2021) 38–50, https://doi.org/10.1039/D0BM01406K.

[11] E.G. Hochreiner, B.G.P. van Ravensteijn, Polymerization-induced self-assembly for drug delivery: A critical appraisal, J. Polym. Sci. 61 (2023) 3186–3210, https://doi.org/10.1002/pol.20230579.

[12] D. Zhou, L. Hu, W. Wang, X. Zhao, Cellular uptake of tailored copolymer synthesized via reversible addition-fragmentation chain transfer (RAFT) polymerization, React. Funct. Polym. 72 (2012) 402–406, https://doi.org/10.1016/j.reactfunctpolym.2012.04.005.

[13] C. Van Bruggen, J.K. Hexum, Z. Tan, R.J. Dalal, T.M. Reineke, Nonviral Gene Delivery with Cationic Glycopolymers, Acc. Chem. Res. 52 (2019) 1347–1358, https://doi.org/10.1021/acs.accounts.8b00665.

[14] Y. Wang, M.J. van Steenbergen, N. Beztsinna, Y. Shi, T. Lammers, C.F. van Nostrum, W.E. Hennink, Biotin-decorated all-HPMA polymeric micelles for paclitaxel delivery, J. Control. Release 328 (2020) 970–984, https://doi.org/10.1016/j.jconrel.2020.09.013.

[15] L. Chan, Y. Huang, T. Chen, Cancer-targeted tri-block copolymer nanoparticles as payloads of metal complexes to achieve enhanced cancer theranosis, J. Mater. Chem. B 4 (2016) 4517–4525, https://doi.org/10.1039/C6TB00514D.

[16] J.V. John, Y.-I. Jeong, R.P. Johnson, C.-W. Chung, H. Park, D.H. Kang, J.K. Cho, Y. Kim, I. Kim, Folic acid-tethered poly(N-isopropylacrylamide)–phospholipid hybrid nanocarriers for targeted drug delivery, J. Mater. Chem. B 3 (2015) 8268–8278, https://doi.org/10.1039/C5TB01063B.

[17] L. Fu, L. Liu, Z. Ruan, H. Zhang, L. Yan, Folic acid targeted pH-responsive amphiphilic polymer nanoparticles conjugated with near infrared fluorescence probe for imaging-guided drug delivery, RSC Adv. 6 (2016) 40312–40322, https://doi.org/10.1039/C6RA05657A.

[18] J.L. Rushworth, K.S. Montgomery, B. Cao, R. Brown, N.J. Dibb, S.K. Nilsson, J. Chiefari, M.J. Fuchter, Glycosylated Nanoparticles Derived from RAFT Polymerization for Effective Drug Delivery to Macrophages, ACS Appl. Bio Mater. 3 (2020) 5775–5786, https://doi.org/10.1021/acsabm.0c00529.

[19] R. De Coen, N. Vanparijs, M.D.P. Risseeuw, L. Lybaert, B. Louage, S. De Koker, V. Kumar, J. Grooten, L. Taylor, N. Ayres, S. Van Calenbergh, L. Nuhn, B.G. De Geest, pH-Degradable Mannosylated Nanogels for Dendritic Cell Targeting, Biomacromolecules 17 (2016) 2479–2488, https://doi.org/10.1021/acs.biomac.6b00685.

[20] A. Corey, K. Stevens, H.-A. Kaur, Self-assembly of protein-polymer conjugates for drug delivery, Adv Drug Deliv Rev 174 (2021) 447–460, https://doi.org/10.1016/j.addr.2021.05.002.

[21] K. Tappertzhofen, M. Bednarczyk, K. Koynov, M. Bros, S. Grabbe, R. Zentel, Toward Anticancer Immunotherapeutics: Well-Defined Polymer–Antibody Conjugates for Selective Dendritic Cell Targeting, Macromol. Biosci. 14 (2014) 1444–1457, https://doi.org/10.1002/mabi.201400190.

[22] B.L. Scotland, A.L. Cottingham, J.J.M. Lasola, S.W. Hoag, R.M. Pearson, Development of Protein–Polymer Conjugate Nanoparticles for Modulation of Dendritic Cell Phenotype and Antigen-Specific CD4 T Cell Responses, ACS Appl. Polym. Mater. 5 (2023) 8794–8807, https://doi.org/10.1021/acsapm.3c00548.

[23] E. Vivès, J. Schmidt, A. Pèlegrin, Cell-penetrating and cell-targeting peptides in drug delivery, Biochim Biophys Acta Rev, Cancer 1786 (2008) 126–138, https://doi.org/10.1016/j.bbcan.2008.03.001.

[24] D.M. Copolovici, K. Langel, E. Eriste, Ü. Langel, Cell-Penetrating Peptides: Design, Synthesis, and Applications, ACS Nano 8 (2014) 1972–1994, https://doi.org/10.1021/nn4057269.

[25] C. Chen, F. Richter, C. Guerrero-Sanchez, A. Traeger, U.S. Schubert, A. Feng, S. H. Thang, Cell-Penetrating, Peptide-Based RAFT Agent for Constructing Penetration Enhancers, ACS Macro Lett 9 (2020) 260–265, https://doi.org/10.1021/acsmacrolett.9b00647.

[26] S. Nooraei, H. Bahrulolum, Z.S. Hoseini, C. Katalani, A. Hajizade, A.J. Easton, G. Ahmadian, Virus-like particles: preparation, immunogenicity and their roles as nanovaccines and drug nanocarriers, J. Nanobiotechnol. 19 (2021) 59, https://doi.org/10.1186/s12951-021-00806-7.

[27] C.L. Jolly, Q.J. Sattentau, Attachment Factors, in: S. Pöhlmann, G. Simmons (eds.) Viral Entry into Host Cells. Adv Exp Med Biol 790 (2006) 1–23. https://doi.org/10.1007/978-1-4614-7651-1_1.

[28] C.J. Russell, M. Hu, F.A. Okda, Influenza Hemagglutinin Protein Stability, Activation, and Pandemic Risk, Trends Microbiol. 26 (2018) 841–853, https://doi.org/10.1016/j.tim.2018.03.005.

[29] M. Akbarian, S.-H. Chen, Instability Challenges and Stabilization Strategies of Pharmaceutical Proteins, Pharmaceutics 14 (2022) 2533, https://doi.org/10.3390/pharmaceutics14112533.

[30] M. Shi, K.J. McHugh, Strategies for overcoming protein and peptide instability in biodegradable drug delivery systems, Adv. Drug Deliv. Rev. 199 (2023) 114904, https://doi.org/10.1016/j.addr.2023.114904.

[31] B.A. Fong, W.-Y. Wu, D.W. Wood, The potential role of self-cleaving purification tags in commercial-scale processes, Trends Biotechnol. 28 (2010) 272–279, https://doi.org/10.1016/j.tibtech.2010.02.003.

[32] J.H. Ko, H.D. Maynard, A guide to maximizing the therapeutic potential of protein–polymer conjugates by rational design, Chem. Soc. Rev. 47 (2018) 8998–9014, https://doi.org/10.1039/C8CS00606G.

[33] N. Sriwilaijaroen, Y. Suzuki, Molecular basis of the structure and function of H1 hemagglutinin of influenza virus, Proc Jpn Acad Ser B 88 (2012) 226–249, https://doi.org/10.2183/pjab.88.226.

[34] M. de Graaf, R.A.M. Fouchier, Role of receptor binding specificity in influenza A virus transmission and pathogenesis, EMBO J. 33 (2014) 823–841, https://doi.org/10.1002/embj.201387442.

[35] S. Ghosh, Sialic acid and biology of life: An introduction, in: Sialic Acids and Sialoglycoconjugates in the Biology of Life, Health and Disease, Elsevier, 2020: pp. 1–61. https://doi.org/10.1016/B978-0-12-816126-5.00001-9.

[36] V.C. Chu, G.R. Whittaker, Influenza virus entry and infection require host cell N-linked glycoprotein, PNAS 101 (2004) 18153–18158, https://doi.org/10.1073/pnas.0405172102.

[37] R.J. Russell, Orthomyxoviruses: Structure of Antigens, in: Encyclopedia of Virology, Elsevier, 2008: pp. 489–494. https://doi.org/10.1016/B978-012374410-4.00431-3.

[38] J.L. Cuellar-Camacho, S. Bhatia, V. Reiter-Scherer, D. Lauster, S. Liese, J.P. Rabe, A. Herrmann, R. Haag, Quantification of Multivalent Interactions between Sialic Acid and Influenza A Virus Spike Proteins by Single-Molecule Force Spectroscopy, J. Am. Chem. Soc. 142 (2020) 12181–12192, https://doi.org/10.1021/jacs.0c02852.

[39] H. Hevekerl, J. Tornmalm, J. Widengren, Fluorescence-based characterization of non-fluorescent transient states of tryptophan – prospects for protein conformation and interaction studies, Sci. Rep. 6 (2016) 35052, https://doi.org/10.1038/srep35052.

[40] A.H. Jesmer, A.S.T. Marple, R.G. Wylie, Controlled swelling of biomaterial devices for improved antifouling polymer coatings, Sci. Rep. 13 (2023) 19950, https://doi.org/10.1038/s41598-023-47192-8.

[41] B. Marco-Dufort, J.R. Janczy, T. Hu, M. Lütolf, F. Gatti, M. Wolf, A. Woods, S. Tetter, B.V. Sridhar, M.W. Tibbitt, Thermal stabilization of diverse biologics using reversible hydrogels, Sci Adv 8 (2022) eabo0502, https://doi.org/10.1126/sciadv.abo0502.

[42] C. Ventura-Hunter, V.D. Lechuga-Islas, J. Ulbrich, C. Kellner, U.S. Schubert, E. Saldívar-Guerra, M. Rosales-Guzmán, C. Guerrero-Sánchez, Glycerol methacrylate-based copolymers: Reactivity ratios, physicochemical characterization and cytotoxicity, Eur. Polym. J. 178 (2022) 111478, https://doi.org/10.1016/j.eurpolymj.2022.111478.

[43] A. Lamiable, P. Thévenet, J. Rey, M. Vavrusa, P. Derreumaux, P. Tufféry, PEP-FOLD3: faster de novo structure prediction for linear peptides in solution and in complex, Nucleic Acids Res. 44 (2016) W449–W454, https://doi.org/10.1093/nar/gkw329.

[44] A. Roy, A. Kucukural, Y. Zhang, I-TASSER: a unified platform for automated protein structure and function prediction, Nat. Protoc. 5 (2010) 725–738, https://doi.org/10.1038/nprot.2010.5.

[45] A.C. Camproux, R. Gautier, P. Tufféry, A hidden Markov model derived structural alphabet for proteins, J. Mol. Biol. 339 (2004) 591–605, https://doi.org/10.1016/j.jmb.2004.04.005.

[46] J. Maupetit, P. Derreumaux, P. Tuffery, PEP-FOLD: An online resource for de novo peptide structure prediction, Nucleic Acids Res. 37 (2009) 498–503, https://doi.org/10.1093/nar/gkp323.

[47] J.T. Pelton, L.R. McLean, Spectroscopic Methods for Analysis of Protein Secondary Structure, Anal. Biochem. 277 (2000) 167–176, https://doi.org/10.1006/abio.1999.4320.

[48] Y. Zhang, I-TASSER (Iterative Threading ASSEmbly Refinement), (2018). https://zhanggroup.org/I-TASSER/ (accessed January 30, 2024).

[49] J. Yu, K. Xiao, W. Xue, Y. xiao Shen, J. Tan, S. Liang, Y. Wang, X. Huang, Excitation-emission matrix (EEM) fluorescence spectroscopy for characterization of organic matter in membrane bioreactors: Principles, methods and applications, Front Environ Sci Eng 14 (2020) 31. https://doi.org/10.1007/s11783-019-1210-8.

[50] R.J. Lamm, E.B. Lim, K.M. Weigandt, L.D. Pozzo, N.J. White, S.H. Pun, Peptide valency plays an important role in the activity of a synthetic fibrin-crosslinking

polymer, Biomaterials 132 (2017) 96–104, https://doi.org/10.1016/j.biomaterials.2017.04.002.
[51] P. Groves, Diffusion ordered spectroscopy (DOSY) as applied to polymers, Polym. Chem. 8 (2017) 6700–6708, https://doi.org/10.1039/c7py01577a.
[52] J. Nguyen, X. Xie, M. Neu, R. Dumitrascu, R. Reul, J. Sitterberg, U. Bakowsky, R. Schermuly, L. Fink, T. Schmehl, T. Gessler, W. Seeger, T. Kissel, Effects of cell-penetrating peptides and pegylation on transfection efficiency of polyethylenimine in mouse lungs, J. Gene Med. 10 (2008) 1236–1246, https://doi.org/10.1002/jgm.1255.
[53] P. Hamm, M.D. Driessen, N. Hauptstein, J. Kehrein, R. Worschech, P. Pouyan, R. Haag, U.S. Schubert, T.D. Müller, L. Meinel, T. Lühmann, Deciphering Polymer Interactions in Bioconjugates with Different Architectures by Structural Analysis via Time-Resolved Limited Proteolysis Mass Spectrometry, Angew. Chem. Int. Ed. (2025) e202415354, https://doi.org/10.1002/anie.202415354.
[54] R. Pérez-Isidoro, F.J. Guevara-Pantoja, C. Ventura-Hunter, C. Guerrero-Sánchez, J. C. Ruiz-Suárez, U.S. Schubert, E. Saldívar-Guerra, Fluidized or not fluidized? Biophysical characterization of biohybrid lipid/protein/polymer liposomes and their interaction with tetracaine, Biochim Biophys Acta Gen Subjects 1867 (2023) 130287. https://doi.org/10.1016/j.bbagen.2022.130287.
[55] R. Pérez-Isidoro, A.G. Valdez-Lara, A.J. Díaz-Salazar, S. Hoeppener, C. Guerrero-Sánchez, P. Quintana-Owen, J.C. Ruiz-Suárez, U.S. Schubert, G. Ayora-Talavera, M.A. De Jesús-Téllez, E. Saldívar-Guerra, Biophysical investigation of liposome systems decorated with bioconjugated copolymers in the presence of amantadine, J. Mater. Chem. B 12 (2024) 5823–5837, https://doi.org/10.1039/D4TB00171K.
[56] R.J. Lamm, T.J. Pichon, F. Huyan, X. Wang, A.N. Prossnitz, K.T. Manner, N. J. White, S.H. Pun, Optimizing the Polymer Chemistry and Synthesis Method of PolySTAT, an Injectable Hemostat, ACS Biomater Sci. Eng. 6 (2020) 7011–7020, https://doi.org/10.1021/acsbiomaterials.0c01189.
[57] N. Cohen, L. Binyamin, Y. Levi-Kalisman, G.Y. Berguig, A. Convertine, P. Stayton, R., Yerushalmi−Rozen, pH and Salt Effects on Surface Activity and Self-Assembly of Copolymers Containing a Weak Polybase, Langmuir 32 (2016) 9286–9292, https://doi.org/10.1021/acs.langmuir.6b02452.
[58] A. Blanazs, A.J. Ryan, S.P. Armes, Predictive Phase Diagrams for RAFT Aqueous Dispersion Polymerization: Effect of Block Copolymer Composition, Molecular Weight, and Copolymer Concentration, Macromolecules 45 (2012) 5099–5107, https://doi.org/10.1021/ma301059r.
[59] Y. Liu, S. Pujals, P.J.M. Stals, T. Paulöhrl, S.I. Presolski, E.W. Meijer, L. Albertazzi, A.R.A. Palmans, Catalytically Active Single-Chain Polymeric Nanoparticles: Exploring Their Functions in Complex Biological Media, J. Am. Chem. Soc. 140 (2018) 3423–3433, https://doi.org/10.1021/jacs.8b00122.
[60] S. Farazi, M.H. Stenzel, R. Chapman, Confinement of folding motifs within central blocks improves single chain polymer nanoparticle folding, Polym. Chem. 15 (2024) 332–340, https://doi.org/10.1039/D3PY01166F.
[61] J.D. Dukes, P. Whitley, A.D. Chalmers, The MDCK variety pack: choosing the right strain, BMC Cell Biol. 12 (2011) 43, https://doi.org/10.1186/1471-2121-12-43.
[62] G. Özhan, Ö.S. Zengin, Z. Seker, A.G. Akyildiz, M. Kara, T. Boran, E. Oztas, P17-27: Role of oxidative stress in microplastic polymethyl methacrylate (PMMA)-induced hepatotoxicity with HepG2/THP-1 co-culture model, Toxicol. Lett. 384 (2023) S217–S218, https://doi.org/10.1016/S0378-4274(23)00768-3.
[63] T. Ramirez, A. Strigun, A. Verlohner, H.-A. Huener, E. Peter, M. Herold, N. Bordag, W. Mellert, T. Walk, M. Spitzer, X. Jiang, S. Sperber, T. Hofmann, T. Hartung, H. Kamp, B. van Ravenzwaay, Prediction of liver toxicity and mode of action using metabolomics in vitro in HepG2 cells, Arch. Toxicol. 92 (2018) 893–906, https://doi.org/10.1007/s00204-017-2079-6.
[64] D.C. Luther, T. Jeon, R. Goswami, H. Nagaraj, D. Kim, Y.-W. Lee, V.M. Rotello, Protein Delivery: If Your GFP (or Other Small Protein) Is in the Cytosol, It Will Also Be in the Nucleus, Bioconjug Chem 32 (2021) 891–896, https://doi.org/10.1021/acs.bioconjchem.1c00103.
[65] D.C. Luther, Y.-W. Lee, H. Nagaraj, V. Clark, T. Jeon, R. Goswami, S. Gopalakrishnan, S. Fedeli, W. Jerome, J.L. Elia, V.M. Rotello, Cytosolic Protein Delivery Using Modular Biotin–Streptavidin Assembly of Nanocomposites, ACS Nano 16 (2022) 7323–7330, https://doi.org/10.1021/acsnano.1c06768.
[66] R. Tréhin, H.M. Nielsen, H.-G. Jahnke, U. Krauss, A.G. Beck-Sickinger, H.P. Merkle, Metabolic cleavage of cell-penetrating peptides in contact with epithelial models: human calcitonin (hCT)-derived peptides, Tat(47–57) and penetratin(43–58), Biochem. J 382 (2004) 945–956, https://doi.org/10.1042/BJ20040238.
[67] C. Foerg, U. Ziegler, J. Fernandez-Carneado, E. Giralt, H.P. Merkle, Differentiation Restricted Endocytosis of Cell Penetrating Peptides in MDCK Cells Corresponds with Activities of Rho-GTPases, Pharm. Res. 24 (2007) 628–642, https://doi.org/10.1007/s11095-006-9212-1.
[68] R. Tréhin, U. Krauss, R. Muff, M. Meinecke, A.G. Beck-Sickinger, H.P. Merkle, Cellular Internalization of Human Calcitonin Derived Peptides in MDCK Monolayers: A Comparative Study with Tat(47-57) and Penetratin(43-58), Pharm. Res. 21 (2004) 33–42, https://doi.org/10.1023/B:PHAM.0000012149.83119.bf.
[69] R. Tréhin, U. Krauss, A.G. Beck-Sickinger, H.P. Merkle, H.M. Nielsen, Cellular Uptake But Low Permeation of Human Calcitonin-Derived Cell Penetrating Peptides and Tat(47-57) Through Well-Differentiated Epithelial Models, Pharm. Res. 21 (2004) 1248–1256, https://doi.org/10.1023/B:PHAM.0000033013.45204.c3.
[70] M. Zheng, J. Yu, The effect of particle shape and size on cellular uptake, Drug Deliv, Transl. Res. 6 (2016) 67–72, https://doi.org/10.1007/s13346-015-0270-y.
[71] R. Augustine, A. Hasan, R. Primavera, R.J. Wilson, A.S. Thakor, B.D. Kevadiya, Cellular uptake and retention of nanoparticles: Insights on particle properties and interaction with cellular components, Mater. Today Commun. 25 (2020) 101692, https://doi.org/10.1016/j.mtcomm.2020.101692.